JOURNAL OF APPLIED PHYSICS VOLUME 95, NUMBER 8 15 APRIL 2004

Comparison of mixed anion, $InAs_yP_{1-y}$ and mixed cation, $In_xAl_{1-x}As$ metamorphic buffers grown by molecular beam epitaxy on (100) InP substrates

M. K. Hudait and Y. Lin
Department of Electrical Engineering, The Ohio State University, Columbus, Ohio 43210

M. N. Palmisiano[a)]
Bechtel Bettis Inc., West Mifflin, Pennsylvania 15122

C. Tivarus and J. P. Pelz
Department of Physics, The Ohio State University, Columbus, Ohio 43210

S. A. Ringel[b)]
Department of Electrical Engineering, The Ohio State University, Columbus, Ohio 43210

(Received 9 October 2003; accepted 16 January 2004)

The structural, morphological, and defect properties of mixed anion, $InAs_yP_{1-y}$ and mixed cation, $In_xAl_{1-x}As$ metamorphic step-graded buffers grown on InP substrates are investigated and compared. Two types of buffers were grown to span the identical range of lattice constants and lattice mismatch (~1.1–1.2%) on (100) InP substrates by solid source molecular beam epitaxy. Symmetric relaxation of ~90% in the two orthogonal ⟨110⟩ directions with minimal lattice tilt was observed for the terminal $InAs_{0.4}P_{0.6}$ and $In_{0.7}Al_{0.3}As$ overlayers of each graded buffer type, indicating nearly equal numbers of α and β dislocations were formed during the relaxation process and that the relaxation is near equilibrium and hence insensitive to asymmetric dislocation kinetics. Atomic force microscopy reveals extremely ordered crosshatch morphology and very low root mean square (rms) roughness of ~2.2 nm for the InAsP relaxed buffers compared to the InAlAs relaxed buffers (~7.3 nm) at the same degree of lattice mismatch with respect to the InP substrates. Moreover, phase decomposition is observed for the InAlAs buffers, whereas InAsP buffers displayed ideal, step-graded buffer characteristics. The impact of the structural differences between the two buffer types on metamorphic devices was demonstrated by comparing identical 0.6 eV band gap lattice-mismatched $In_{0.69}Ga_{0.31}As$ thermophotovoltaic (TPV) devices that were grown on these buffers. Clearly superior device performance was achieved on $InAs_yP_{1-y}$ buffers, which is attributed primarily to the impact of layer roughness on the carrier recombination rates near the front window/emitter interface of the TPV devices. © *2004 American Institute of Physics.*
[DOI: 10.1063/1.1667006]

I. INTRODUCTION

Compositionally graded metamorphic buffers are of great interest since they offer an approach to alter the substrate lattice constant to a desired value for a given device application. For cubic III–V and IV–IV semiconductors, these buffer layers relax misfit strain primarily by the formation of 60° $a/2\langle 110\rangle\{111\}$ misfit dislocations (MDs) at layer interfaces, which via dislocation glide can accommodate lattice mismatch between the substrate and mismatched device layer. This technique has been utilized to produce relaxed, "virtual" substrates for many applications, including SiGe-based heterojunction field effect transistors,[1] $In_xGa_{1-x}As/GaAs$ light emitting diodes (LEDs),[2] $In_xGa_{1-x}P/GaP$ LEDs,[3] $In_xGa_{1-x}P/GaAs$ metamorphic heterojunctions bipolar transistors,[4] $In_xGa_{1-x}P/GaAs$,[5–8] $In_xAl_{1-x}As/In_xGa_{1-x}As$ high electron mobility transistors on GaAs,[9–11] and $GaAs/Ge/Si_{1-x}Ge_x/Si$ solar cells.[12] Recently, low band gap, $In_xGa_{1-x}As$-based thermophotovoltaic (TPV) devices, which are receiving substantial interest for energy conversion applications, are also exploiting metamorphic buffers to reach the band gap range of interest, 0.5–0.6 eV for InGaAs devices on InP. To date, several groups have successfully applied $InAs_yP_{1-y}$ compositionally graded buffers on InP substrates for this purpose.[13–17] However, $In_xAl_{1-x}As$, a very well known compound successfully used in several other device technologies, also happens to span the same lattice constant range that can bridge InP substrates to 0.5–0.6 eV band gap $In_xGa_{1-x}As$ TPV devices. Hence, one purpose of this article is to investigate and compare the growth, structural, and morphological properties of $InAs_yP_{1-y}$ and $In_xAl_{1-x}As$ metamorphic buffers grown by molecular beam epitaxy (MBE) on InP and evaluate their relative applicability to lattice-mismatched, relaxed $In_xGa_{1-x}As$ TPV devices. An additional, more fundamen-

---

[a)] Present address: ANH Refractories Company, Technology Center, 1001 Pittsburgh-McKeesport Blvd., West Mifflin, PA 15122.

[b)] Author to whom correspondence should be addressed; electronic mail: ringel@ee.eng.ohio-state.edu tally motivating factor for this study stems from the use of a group-V, anion-based graded alloy, $InAs_yP_{1-y}$, as opposed to a graded cation alloy, $In_xAl_{1-x}As$, for the purpose of grading the substrate lattice constant. The use of a graded anion buffer, $InAs_yP_{1-y}$ for MBE growth offers a potential advantage compared with the more common graded buffers such as $In_xGa_{1-x}As$ and $In_xAl_{1-x}As$, since control of the growth rate (indium flux) for the former is decoupled from control of the layer composition and hence lattice constant. This provides an additional degree of freedom when attempting to optimize strain relaxation in these material systems.

II. EXPERIMENTAL DETAILS

A. Growth of $In_xAl_{1-x}As$ step-graded buffers

$In_xAl_{1-x}As$ layers ($x=0.52-0.70$) were grown on semi-insulating (100) InP substrates starting with a lattice-matched composition of $In_{0.52}Al_{0.48}As$ and subsequent grading to higher In content using solid source MBE. Substrate oxide desorption was done at 510 °C under a phosphorus overpressure of $\sim 1\times 10^{-5}$ Torr, which was verified by a strong (2×4) reflection high-energy electron diffraction (RHEED) pattern, indicative of an oxide-free (100) InP surface. An initial 0.2 μm thick undoped InP buffer layer was then deposited to generate a smooth surface at ~485 °C under a stabilizing P_4 flux prior to the growth of $In_xAl_{1-x}As$ step-graded buffers. The initial (2×4) symmetry on the (100) InP surface observed by RHEED became slightly blurry, but clearly observable, as a function of $In_xAl_{1-x}As$ growth time. The In and Al fluxes were independently varied to achieve the step grade while maintaining a constant growth rate of ~3.28 Å/s throughout the growth. The growth temperature was monotonically reduced from 520 to 505 °C in order to suppress In droplets for the high In content layers and a spotty RHEED pattern. Details of the growth temperature profile are discussed in Sec. III A 1. An As_2/III ratio of 24 was maintained at all times. The first three, unintentionally doped (uid) layers of the step-graded buffers were each grown to a thickness of 0.4 μm with nominal compositions of $In_{0.52}Al_{0.48}As$, $In_{0.58}Al_{0.42}As$, and $In_{0.64}Al_{0.36}As$, followed by a final 1.5 μm thick uid $In_{0.7}Al_{0.3}As$ layer. For cross-sectional transmission electron microscopic (TEM) study, a final $In_{0.69}Ga_{0.31}As$ overlayer was grown to be lattice matched to the final $In_{0.7}Al_{0.3}As$ layer, resulting in a total lattice mismatch of ~1.1%–1.2%.

B. Growth of $InAs_yP_{1-y}$ step-graded buffers

$InAs_yP_{1-y}$ layers ($y=0.05-0.50$) were grown on semi-insulating (100) InP substrates after the growth of 0.2 μm thick undoped InP buffer under a stabilizing P_4 flux with an average grading rate of 20% As/μm. The P_4/In ratio was fixed at 7/1 during the $InAs_yP_{1-y}$ growth at a growth temperature of 485 °C.[18] These values for the P_4/In ratio and the growth temperature of 485 °C were selected based on Hall mobility and low temperature photoluminescence results from series of *n*-type InP samples grown at different P_4/In ratios. The exposure time of As_2 on the InP surface was minimized prior to $InAs_yP_{1-y}$ growth, in order to avoid the formation of an InAsP interlayer due to As–P exchange on the InP surface.[19,20] A strong (2×4) RHEED pattern was consistently observed throughout the $InAs_yP_{1-y}$ growth. The growth rate and the growth temperature for all the $InAs_yP_{1-y}$ layers were kept constant at 0.75 monolayers per second (ML/s), as determined by RHEED intensity oscillations and ~485 °C, respectively. The first three, undoped step-graded layers were each grown to a thickness of 0.4 μm, followed by a final 1.5 μm thick $InAs_{0.4}P_{0.6}$ layer. Similar to the InAlAs buffers, the total mismatch of the entire heterostructure was nominally 1.1%–1.2%.

C. Structural characterization and relaxation calculation for graded buffers

The strain relaxation, surface morphology, and defect properties of the step-graded buffers were characterized using triple axis x-ray diffraction (TAXRD), Nomarski microscopy, atomic force microscopy (AFM), plan-view TEM, and cross-sectional TEM (XTEM). TEM samples were prepared by a conventional mechano-chemical thinning procedure followed by Ar ion milling. XRD measurements were carried out with a Bede Scientific Instruments D1 system using the Cu K_{α_1} line. Rocking curves ($\omega-2\theta$ scan) and the reciprocal space maps (RSMs) were obtained. Since MDs relieve epilayer strain, an asymmetry in MD density should result in different in-plane lattice mismatches in the two orthogonal $[110]$ and $[1\bar{1}0]$ directions. Two sets of RSMs, the symmetric (004) and asymmetric (115), were measured in order to determine the alloy composition, lattice mismatch, and residual strain, in each $\langle 110\rangle$ in-plane direction. With these data, the epilayer can be characterized by three misfit parameters, $(\Delta a/a)_\perp$, $(\Delta a/a)\|_{[1\bar{1}0]}$, and $(\Delta a/a)\|_{[110]}$. The relaxed misfit can then be calculated from[21–23]

$$\left(\frac{\Delta a}{a}\right)_r=\frac{1-\nu}{1+\nu}\left(\frac{\Delta a}{a}\right)_\perp+\frac{\nu}{1+\nu}\times\left[\left(\frac{\Delta a}{a}\right)\bigg\|_{[1\bar{1}0]}+\left(\frac{\Delta a}{a}\right)\bigg\|_{[110]}\right], \qquad (1)$$

where ν is Poisson's ratio of each ternary layer calculated from the elastic constants of GaAs, InAs, and InP using Vegard's law,[24] $(\Delta a/a)_\perp$ is the perpendicular misfit, and $(\Delta a/a)\|_{[1\bar{1}0]}$ and $(\Delta a/a)\|_{[110]}$ are the in-plane misfits measured with the projection of the incident beam oriented along the $[1\bar{1}0]$ and $[110]$ directions, respectively. Equation (1) applies to the most general case of orthorhombic, tetragonal, and cubic symmetry. From these terms, the net strain and the relaxation in each $\langle 110\rangle$ direction can be expressed as[22,23]

$$R_{[110]}=\frac{\left(\frac{\Delta a}{a}\right)\Big\|_{[110]}}{\left(\frac{\Delta a}{a}\right)_r}$$

and

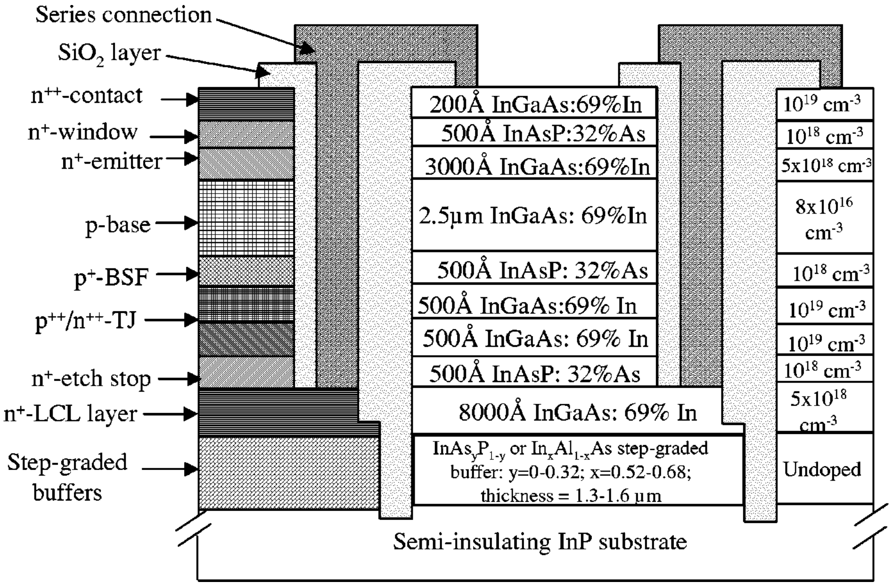

FIG. 1. Schematic cross section of a typical lattice-mismatched $In_{0.69}Ga_{0.31}As$ $n/p/n$ TPV test structure using either $InAs_yP_{1-y}$ or $In_xAl_{1-x}As$ step-graded buffers (Ref. 13). Nominal composition and doping are shown.

$$R_{[1\bar{1}0]}=\frac{\left(\frac{\Delta a}{a}\right)\Big\|_{[1\bar{1}0]}}{\left(\frac{\Delta a}{a}\right)_r}. \tag{2}$$

For symmetric relaxation where $R_{[110]}=R_{[1\bar{1}0]}$, Eq. (2) reduces to the conventional definition of relaxation and the average relaxation is $\bar{R}=(R_{[110]}+R_{[1\bar{1}0]})/2$.

D. Growth and processing of single junction (SJ) TPV devices

In certain cases, SJ lattice-mismatched $In_{0.69}Ga_{0.31}As$ TPV devices with band gaps of 0.6 eV were grown and processed on both cation and anion-mixed step-graded buffers to compare the impact of anion and cation buffers on device characteristics. For this application, step-graded $InAs_yP_{1-y}$ and $In_xAl_{1-x}As$ buffer layers with the final composition of $InAs_{0.32}P_{0.68}$ and $In_{0.68}Al_{0.32}As$, respectively, were used to mitigate the effects of the lattice mismatch between the $In_{0.69}Ga_{0.31}As$ device layer and the InP substrate and provide a nominally lattice matched virtual substrate for the $In_{0.69}Ga_{0.31}As$ TPV devices. The schematic cross section of the fully processed $n/p/n$ TPV structure used in this work is shown in Fig. 1 and follows conventional TPV monolithic interconnected module design.[13] Details of this device design can be found elsewhere and is beyond the scope of this article.[13–15] Conventional Ti/Au (200 Å/3 μm) metallization was used for both front and back ohmic contacts. A sputter deposited SiO_2 dielectric layer was used to prevent the interconnect metallization from short circuiting the individual cells. No intentional antireflection coating (ARC) was deposited on the top surface and the heavily doped $In_{0.69}Ga_{0.31}As$ cap layer was removed prior to performing quantum efficiency measurements.

III. EXPERIMENTAL RESULTS

A. Structural properties

1. Temperature stability during growth

Control of the surface temperature during growth is crucial to control alloy composition and obtain good surface morphology. For MBE, this is complicated by the fact that the optimum growth temperature depends on the desired As composition in $InAs_yP_{1-y}$ alloys and the In composition in $In_xAl_{1-x}As$ layer, and the actual temperature is influenced by both the presence of hot effusion cells and emissivity variation from the semi-insulating InP substrates to the epilayers. To account for these issues and to maintain reproducibility, an optical pyrometer-based feedback control loop was used to adjust the substrate temperature in real time to maintain the desired surface temperature during growth. Examples of measured surface temperature profiles for $InAs_{0.4}P_{0.6}/InAs_yP_{1-y}/InP$ and $In_{0.7}Al_{0.3}As/In_xAl_{1-x}As/InP$ runs are shown in Fig. 2. As shown, the growth temperature was intentionally decreased for each step of increased In content for the $In_xAl_{1-x}As$ layers in order to maintain good surface quality. Note that while $In_xAl_{1-x}As$ can be grown at much lower temperatures,[25,26] we chose to work at the maximum growth temperatures without degrading the surface in order to enhance strain relaxation in these mismatched structures. The impact of the growth steps between the step-graded layers to adjust the In and Al fluence between each layer to maintain a constant growth rate and growth temperature is clear from the short dips in measured surface temperature profiles. The surface temperature profile for the first three $In_xAl_{1-x}As$ steps is very smooth, with the slight, uniform decrease within each step attributed to the increasingly efficient heating of the growing epilayers. In contrast, the final, thicker step shows ~10–20 °C fluctuation, which may be due to the effect of surface roughening on light scattering sensed by the pyrometer.

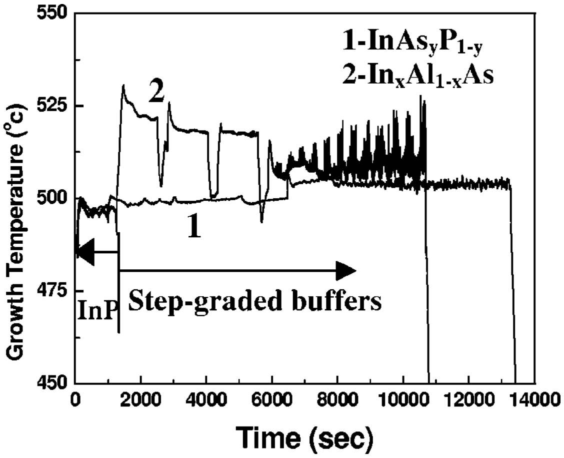

FIG. 2. Surface temperature profiles measured in real time by optical pyrometry for InAs$_y$P$_{1-y}$ and In$_x$Al$_{1-x}$As step-graded buffers. The surface temperature was decreased slowly with increasing In composition for the In$_x$Al$_{1-x}$As layers by adjusting the substrate heater. The growth time was different for these step-graded buffers, since InAsP and InAlAs growth rate were 2.2 and 3.28 Å/s, respectively, however, the total thicknesses of step-graded buffers are identical.

In contrast to In$_x$Al$_{1-x}$As graded buffers, the anion-based InAs$_y$P$_{1-y}$ step grades displayed virtually no scatter in measured surface temperature, suggesting improved (smoother) surface morphology. For these structures, the nominal growth temperature was kept constant for the entire structure since the In flux, and thus In content in the buffer and the growth rate, is never varied. This allowed us to generate a calibration curve for the As:P ratio for InAsP growth at a single temperature, which is necessary since As$_2$ and P$_4$ have nonunity temperature-dependent sticking coefficients. As described earlier, a P$_4$/In flux ratio of 7 was used, and the As$_2$ flux was systematically varied to develop the calibration curve shown in Fig. 3, which was obtained using TAXRD measurements. As seen from Fig. 2, there are virtually no short-range temperature excursions and the fluctuation in surface temperature over several microns of growth is less than 5 °C. It should be noted that while the nominal growth temperature was ~485 °C, the measured temperature profile was within the range of 495–504 °C due to reflected light from opening of the In source during growth.

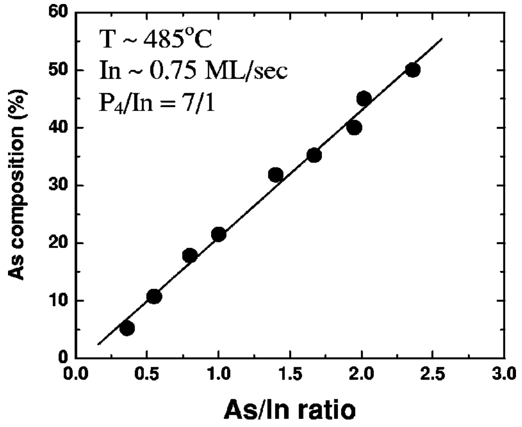

FIG. 3. As content as a function of As/In flux ratios in InAs$_y$P$_{1-y}$ layers as determined by triple axis x-ray diffraction.

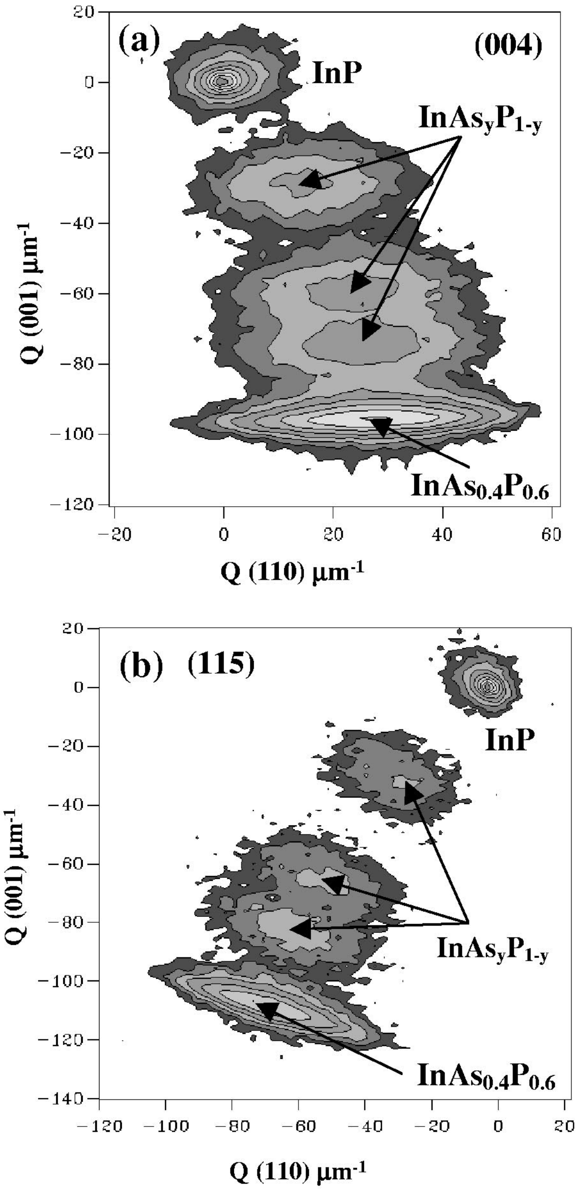

FIG. 4. (a) Symmetric (004) and (b) asymmetric (115) reciprocal space maps of an InAs$_{0.4}$P$_{0.6}$ layer grown on a three-step InAs$_y$P$_{1-y}$ graded buffer obtained using a incident beam along the [110] direction.

2. Strain relaxation properties

The relaxation state and the residual strain of each buffer were measured using RSMs obtained from both symmetric (004) and asymmetric (115) reflections. Figure 4 shows RSMs obtained from a 1.5 μm thick InAs$_{0.4}$P$_{0.6}$ epitaxial layer on a three-step InAs$_y$P$_{1-y}$ buffer on an (001) InP substrate with the incident beam along the [110] direction. From RSMs, one can calculate the degree of relaxation of the overlayer, the two orthogonal $\langle 110\rangle$ lattice parameters in the growth plane $a_{\parallel}$, and the lattice parameter in the growth direction $a_{\perp}$. The relaxation R and the residual strain ε^r in the two orthogonal $\langle 110\rangle$ directions within each layer were determined using Eqs. (2) and (3)[27,28]

$$\varepsilon' = (a_{\text{layer}} - a_{\parallel})/a_0, \tag{3}$$

where a_{layer} is the relaxed layer lattice constant and a_0 is the lattice parameter of the InP substrate. Using RSMs from Figs. 4(a) and 4(b), the measured lattice constants along perpendicular and parallel directions of the top $InAs_{0.4}P_{0.6}$ layer were found to be 5.9523 and 5.9419 Å, respectively. The degree of relaxation of the $InAs_{0.4}P_{0.6}$ layer was found to be more than 90% by using Eqs. (1) and (2) along with the measured values of in-plane and perpendicular lattice constants, leaving a residual strain of ~0.1%, noting a relative experimental error of ±3%. This level of relaxation is consistent with the thickness of the cap layer being well in excess of critical thickness, and indicates efficient relaxation of the 1.2% total misfit strain.

The $In_xAl_{1-x}As$ step-graded buffers show a similar amount of relaxation. Using the lattice parameters extracted from the RSMs shown in Fig. 5 for the (004) and (115) reflections of a 1.5 μm thick $In_{0.7}Al_{0.3}As$ layer grown on a three-step $In_xAl_{1-x}As$ step-graded buffer, the relaxation of the final $In_{0.7}Al_{0.3}As$ layer was calculated to be ~87%, leaving a residual strain of ~0.15%. The corresponding measured lattice constants along perpendicular and parallel directions of the top $In_{0.7}Al_{0.3}As$ layer were found to be 5.9438 and 5.9266 Å, respectively.

Symmetric relaxation of ~90% was observed along the two $[110]$ and $[1\bar{1}0]$ directions in the $InAs_{0.4}P_{0.6}$ layer, indicating isotropic relaxation by similar total MD length in both directions. Since in III–V heterostructures, plastic relaxation occurs mainly via the misfit component of a 60° dislocation, relaxation in the $[110]$ direction is controlled by the nucleation and glide of α dislocations, and relaxation along the $[1\bar{1}0]$ direction is controlled by the nucleation and glide of β dislocations. The different core structures of α and β dislocations can lead to significant differences in activation energies for dislocation nucleation and glide.[28–30] This chemical difference of the dislocation's core structure has been suggested to be responsible for often-observed anisotropy of optical, electrical, and mechanical properties of III–V compound semiconductor materials,[28–30] in addition to anisotropies for devices fabricated in the $[110]$ and $[1\bar{1}0]$ in-plane directions.[23,31,32] Here, since almost equal numbers of α and β dislocations are formed during the relaxation process of the $InAs_{0.4}P_{0.6}$ layer, this symmetry suggests that the relaxation is near equilibrium and hence insensitive to asymmetric dislocation kinetics. It should be noted, however, that other studies on $InAs_yP_{1-y}$ have reported asymmetric strain relaxation in orthogonal $\langle 110\rangle$ directions, but these involved highly mismatched interfaces without step-graded buffers.[33–35] For such interfaces, strain relaxation becomes heavily influenced by MD nucleation kinetics, in addition to dislocation–dislocation interactions.[36] Finally, for the case of graded $In_xAl_{1-x}As$, the strain relaxation was also found to be symmetric with a relaxation of ~87% along the two orthogonal $\langle 110\rangle$ directions. It can be concluded that the relaxation of step-graded $InAs_yP_{1-y}$ anion-based and $In_xAl_{1-x}As$ cation-based buffers on (100) InP substrates are not nucleation limited for this growth regime and degree of lattice mismatch.

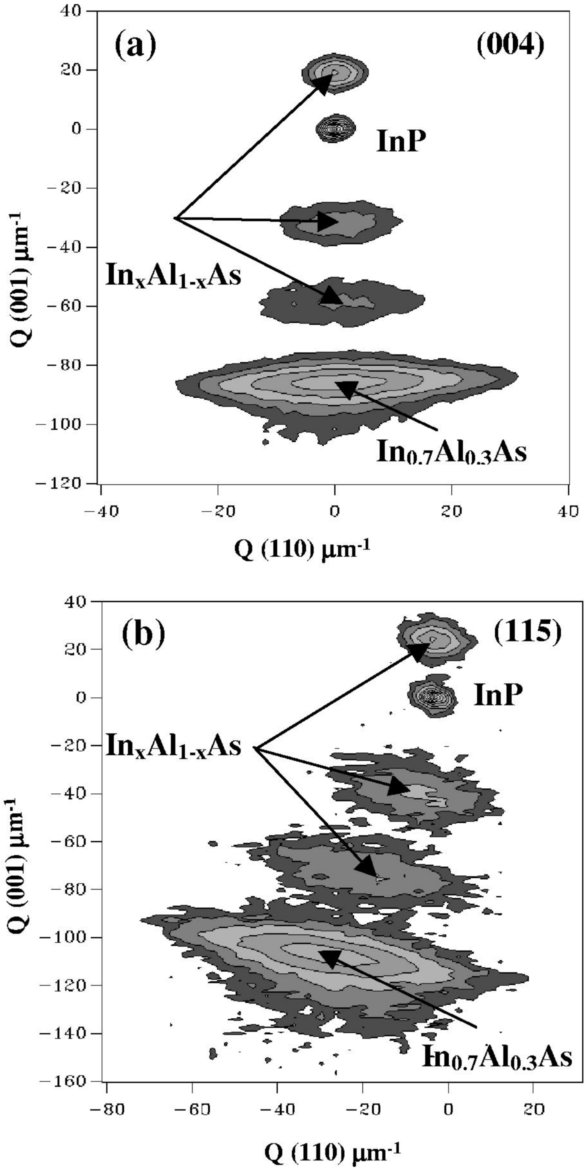

FIG. 5. (a) Symmetric (004) and (b) asymmetric (115) reciprocal space maps of an $In_{0.7}Al_{0.3}As$ layer grown on a three-step $In_xAl_{1-x}As$ graded buffer obtained using a incident beam along the $[1\bar{1}0]$ direction.

Symmetric relaxation of $InAs_{0.4}P_{0.6}$ and $In_{0.7}Al_{0.3}As$ suggests that the magnitude of the epilayer tilt with respect to the substrate will be minimal. If the epilayer is tilted with respect to the substrate, the XRD peak separation between the substrate and the epilayer will vary sinusoidally as a function of azimuthal angle of the incoming x ray,[37] with the magnitude of the sine function indicating the degree of tilt. Here, very small tilt angles, within the range of 25–190 arcsec, were measured as a function of azimuthal angle for both $InAs_{0.4}P_{0.6}$ and $In_{0.7}Al_{0.3}As$ layers with respect to the (001) InP substrate. This small lattice tilt amplitude (noting that tilt up to 2800 arcsec has been reported for other III–V related layers on (001) substrates)[38–41] indicates a nearly equal amount of α and β dislocations participate during the relaxation process, consistent with the observed symmetry in strain relaxation. Note while it is possible that lattice tilt can also be induced by other mechanisms, the lack of tilt ob-

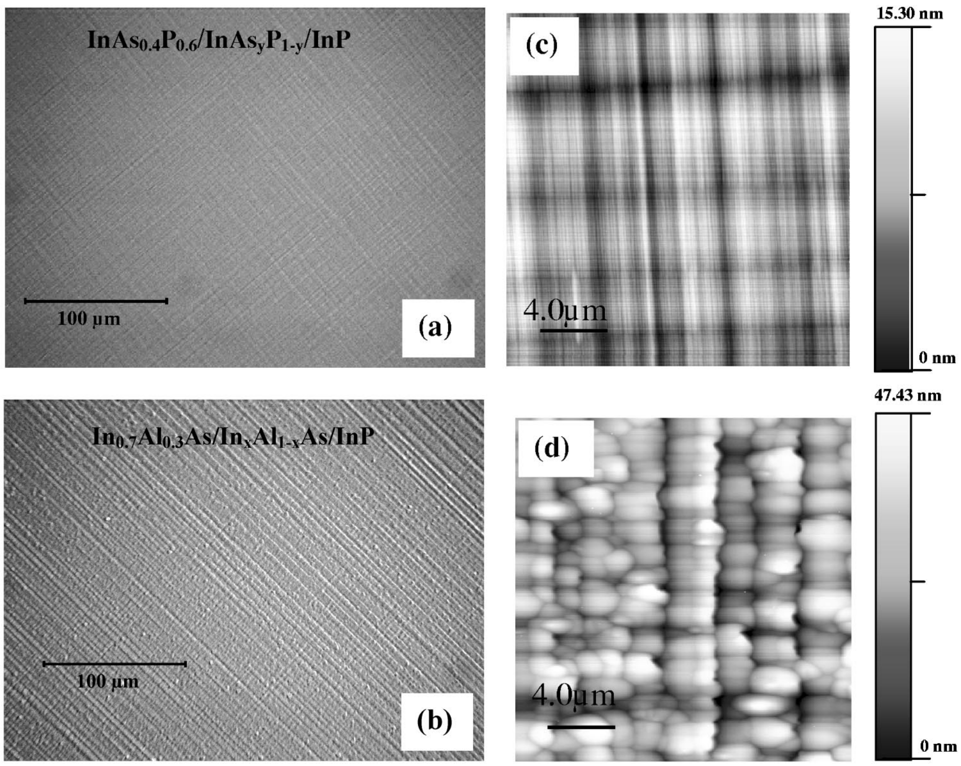

FIG. 6. Nomarski microscopy images of (a) $InAs_{0.4}P_{0.6}$ and (b) $In_{0.7}Al_{0.3}As$, and high-resolution AFM images of (c) $InAs_{0.4}P_{0.6}$ and (d) $In_{0.7}Al_{0.3}As$ layers grown on InP substrates using $InAs_yP_{1-y}$ and $In_xAl_{1-x}As$ graded buffers, respectively.

served here indicates that these mechanisms are suppressed for our growth conditions. Were there a preferential nucleation of one kind of dislocation (either α or β), the film would have displayed much larger tilt magnitude, as has been reported for many lattice-mismatched material systems.[28,30,38,39]

3. Surface morphology and dislocations

The most obvious physical difference between the cation and anion metamorphic buffers is in the surface morphology. The Nomarski images of the relaxed $InAs_{0.4}P_{0.6}$ and $In_{0.7}Al_{0.3}As$ surfaces are shown in Figs. 6(a) and 6(b), respectively. From Fig. 6(a), one can see a well-developed, extremely uniform two-dimensional crosshatch pattern for the InAsP, as expected for an ideal graded buffer. The InAlAs morphology also displays a strong two-dimensional crosshatch pattern but closer observation reveals a grainy texture dispersed across the surface. The AFM images in Figs. 6(c) and 6(d) provide a clearer and quantifiable picture of the differences. The root mean square (rms) surface roughness for the relaxed InAsP buffer is ~2.2 nm as opposed to ~7.3 nm for the relaxed $In_{0.7}Al_{0.3}As$ buffer. This is consistent with RHEED observation during growth, which displayed a more streaky (2×4) surface reconstruction pattern for InAsP, and is also consistent with the differences in the pyrometer traces of Fig. 2, where the scatter in apparent surface temperature for the upper part of the InAlAs growth is attributed to light scattering from the rougher relaxed InAlAs surface. The source for the InAlAs roughness may be the different surface mobilities of In and Al adatoms that can cause randomized nucleation during InAlAs layers, which becomes more apparent with increasing In content.[38] This mechanism of roughening would not be present for InAsP, since only one group-III component, In, is present.

Further insight into the structural differences between cation-graded InAlAs versus anion-graded InAsP buffers are revealed by TEM. Figure 7(a) shows a representative XTEM image of a relaxed $InAs_{0.4}P_{0.6}$ layer grown on InP substrate using $InAs_yP_{1-y}$ graded buffers. The composition and thickness of each layer are indicated in this figure. This XTEM image shows high contrast at the graded buffer layer interfaces due to MDs with no threading dislocations (TDs) observable in the $InAs_{0.4}P_{0.6}$ cap layer at this scale. This conservatively indicates that the threading dislocation density (TDD) in this $InAs_{0.4}P_{0.6}$ layer is below 10^7 cm^{-2}. More accurate TD counting has been performed using plan-view TEM, which shows an average TDD of $\sim4\times10^6$ cm^{-2} for this film.[18] In contrast, XTEM images of a representative InAlAs-based graded structure, Fig. 7(b), show clearly observable defects at this scale that are not simple TDs and instead appear to be the onset of phase decomposition taking place in the final $In_{0.68}Al_{0.32}As$ buffer layer. The presence of phase decomposition here is consistent with the observation of an increase in InAlAs surface roughness during (by RHEED and pyrometry) and after (by AFM) growth. This correlation between phase decomposition and surface roughening may be reasonable since both are linked by the different bond strengths between In–As (1.41 eV) and Al–As (1.98 eV),[42] which leads to varying formation energies and group III adatom mobilities, respectively. Indeed, such a correlation has been previously noted for MBE-grown InAlAs alloys on InP where roughness and spinodal decomposition were linked in a direct fashion.[43,44] While a more in depth study of this correlation is in order, the impact of the struc-

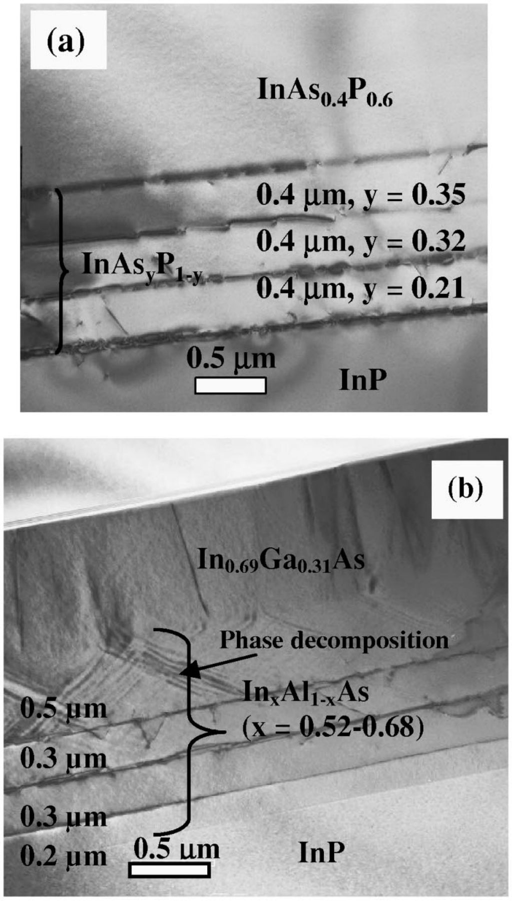

FIG. 7. Cross-sectional TEM images of (a) an $InAs_{0.4}P_{0.6}$ layer grown on a step-graded $InAs_yP_{1-y}$/InP substrate and (b) an $In_{0.69}Ga_{0.31}As$ layer grown on a step-graded $In_xAl_{1-x}As$/InP substrate.

tural differences between the anion (InAsP) and cation (InAlAs) graded buffers on lattice matched, metamorphic InGaAs overlayers are clear from Fig. 7. As seen in Fig. 7(b), extended regions of phase decomposition are observed within the InGaAs overlayer using the InAlAs buffers, which is not present for InGaAs layers on the InAsP buffers. One can expect a profound influence of these microstructural differences on subsequently fabricated metamorphic InGaAs devices. The next section explicitly compares the impact of buffer type on test devices for this study.

B. Comparison of metamorphic TPV devices on cation and anion grades

1. *Current–voltage (I–V) characteristics of SJ* $In_{0.69}Ga_{0.31}As$ *TPV devices*

In order to assess what impact the differences between the graded cation and anion buffers may have on subsequent devices, we grew, fabricated, tested, and compared basic SJ thermophotovoltaic devices following the structure shown in Fig. 1, with no attempt of optimization. Figure 8 shows current density versus voltage ($J-V$) results obtained from identical SJ TPV cells under high-intensity, low emissivity white light illumination as a function of buffer type. The light source used is a quartz halogen tungsten lamp with a spectral emission that fits a graybody 2050 K spectrum with an emissivity of 0.0252. Short-circuit current density (J_{sc}) and open-circuit voltage (V_{oc}) values of 1.18 A/cm^2 and 357 mV, respectively, were obtained for SJ devices grown on $InAs_yP_{1-y}$ graded buffers compared with values of 1.05 A/cm^2 and 274 mV obtained for SJ devices on $In_xAl_{1-x}As$ graded buffers measured under identical conditions. The significantly superior device performance using the InAsP anion buffers clearly tracks the material quality that was described in earlier sections. The measured V_{oc} of 357 mV is comparable to the theoretically predicted V_{oc} value of 380 mV expected for a basic $In_{0.69}Ga_{0.31}As$ p/n junction with a band gap of 0.6 eV, as described in Ref. 45. Details on MBE TPV device performance can be found in Ref. 13.

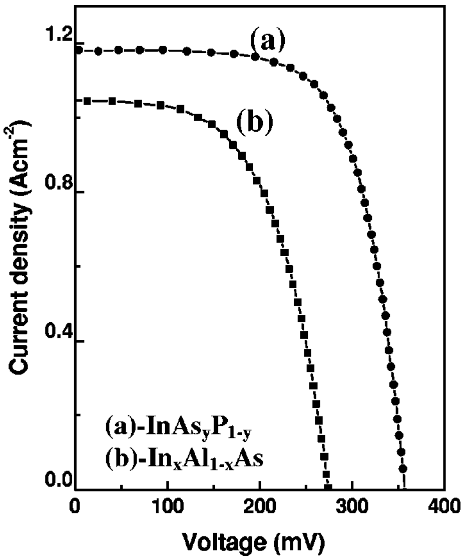

FIG. 8. Current density vs voltage ($J-V$) characteristics of identical $In_{0.69}Ga_{0.31}As$ single junction TPV cells grown on: (a) $InAs_yP_{1-y}$/InP and (b) $In_xAl_{1-x}As$/InP substrates. The light source is a quartz halogen tungsten lamp with a 2050 K graybody spectrum and an emissivity of 0.0252.

Further differences between the characteristics of these devices are shown by Fig. 9, which plots the V_{oc} measured as

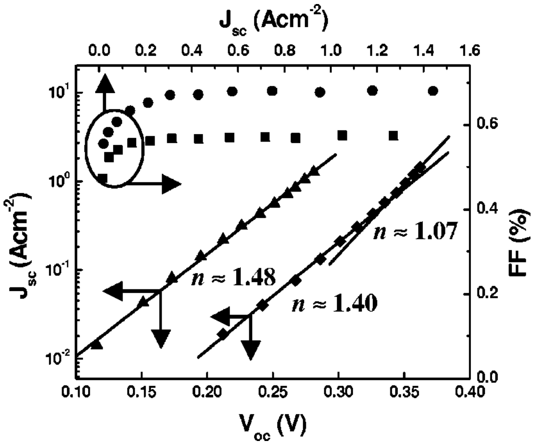

FIG. 9. Plots of $J_{sc}-V_{oc}$ and FF$-J_{sc}$ for identical $In_{0.69}Ga_{0.31}As$ single junction TPV cells grown on $InAs_yP_{1-y}$/InP (●), (◆) and $In_xAl_{1-x}As$/InP (■), (▲) substrates as a function of incident light intensity. Fitted values for the diode ideality factors obtained by regression analysis of the $J_{sc}-V_{oc}$ data for each device are indicated.

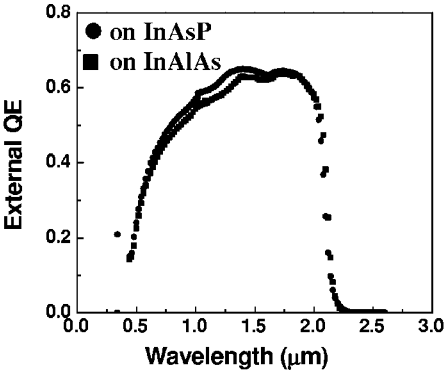

FIG. 10. External quantum efficiency (without AR coating) for identical $In_{0.69}Ga_{0.31}As$ single junction TPV cells grown on $InAs_yP_{1-y}/InP$ (●) and $In_xAl_{1-x}As/InP$ (■) substrates.

a function of J_{sc} and the fill factor as a function of J_{sc}. Here, J_{sc} is controlled by varying the illumination intensity during $J-V$ measurements. In both cases, the maximum obtainable J_{sc} is limited by the output of our lamp. Several features are immediately notable. First, for the range of illumination intensities used here, the $\log(J_{sc})-V_{oc}$ behavior for the lattice mismatched $In_{0.69}Ga_{0.31}As$ TPV device on $InAs_yP_{1-y}/InP$ shows two distinct linear regions, with a diode ideality factor of $n \sim 1.40$ for V_{oc} values below ~330 mV that switches to $n \sim 1.07$ for $V_{oc} > 330$ mV obtained via regression analysis. This indicates the onset of near ideal minority carrier injection/diffusion transport as the dominant current mechanism through the V_{oc} point used in Fig. 9 as would be expected for low defect density material. In contrast, the TPV device grown on graded $In_xAl_{1-x}As/InP$ shows a single slope with $n \sim 1.48$ over the same range of current values, suggesting that a defect-mediated current mechanism such as depletion region recombination plays a more dominant role in these devices. Second, higher V_{oc} values at every J_{sc} value for the device on the $InAs_yP_{1-y}/InP$ substrate are apparent, which is attributed to much lower values of the dark diode saturation current density, J_0, for the $In_{0.69}Ga_{0.31}As$ device on $InAs_yP_{1-y}/InP$. Numerical analysis of the $J_{sc}-V_{oc}$ data indicates that J_0 increases from a value of 2.7 $\mu A/cm^2$ for the device on $InAs_yP_{1-y}/InP$ to 796 $\mu A/cm^2$ for the device on $In_xAl_{1-x}As/InP$, an increase by almost a factor of 300. The variation in fill factor (FF) with J_{sc} showed similar trends, with a maximum FF of 68.1% for TPV devices on $InAs_yP_{1-y}/InP$ as compared to 57.5% for TPV devices on $In_xAl_{1-x}As$ graded buffers, respectively, indicating the close correlation between the structural quality of the metamorphic material and device performance.

2. External quantum efficiency of SJ $In_{0.69}Ga_{0.31}As$ TPV devices

External quantum efficiency (EQE) measurements were used to qualitatively investigate which regions of the TPV devices may be most affected by the graded buffers in this study. Figure 10 compares the EQE curves of SJ TPV cells grown on $InAs_yP_{1-y}$ and $In_xAl_{1-x}As$ step-graded buffers. All demonstrated high collection efficiency. An approximately uniform EQE of ~65% is observed in the wavelength of 1200–2000 nm without the benefit of an ARC that would typically increase this by ~25%–30% absolute.[46] This illustrates the effectiveness of the $In_{0.69}Ga_{0.31}As$ p/n junction in collecting carriers from both the base/back surface field interface region and throughout the base layer, implying that the electron minority carrier diffusion length is in excess of the 2.5 μm base thickness, using either buffer material in spite of the different defect structures and interfaces. One can conclude from this that the defect density, while higher for InGaAs grown on InAlAs, is still below a critical threshold so that it does not limit the carrier diffusion length to a first order. However, the same cannot be concluded for the shorter wavelength region, which is more sensitive to recombination in the upper device layers. Here, the EQE is reduced for devices on $In_xAl_{1-x}As$ buffers. The lower EQE in this range implies poor collection from the emitter layer, which can be attributed to a higher recombination velocity at the InAsP/InGaAs window/emitter interface, presumably due to the increased layer roughness for devices on InAlAs buffers. A large interface recombination velocity can be expected to substantially increase J_0 and lower V_{oc} values. In addition, a lower overall EQE will lead to reduced J_{sc} value. This is consistent with the experimental observations described above. Hence, the device results and analysis are themselves consistent with the different material properties for the two fundamentally different types of buffers as described earlier in this article.

IV. CONCLUSIONS

We have compared the structural, morphological, and growth properties of relaxed, step-graded $InAs_yP_{1-y}$ and $In_xAl_{1-x}As$ epitaxial layers on InP substrates grown by solid source MBE. Both anion-based and cation-based buffer types displayed a high degree of symmetric relaxation with minimal lattice tilt for the final $InAs_{0.4}P_{0.6}$ and $In_{0.7}Al_{0.3}As$ overlayers. This revealed very similar numbers of α and β dislocations were formed during the relaxation process for both buffer types. AFM displayed extremely ordered crosshatch morphology and very low rms roughness of ~2.2 nm for $InAs_yP_{1-y}$ graded buffers compared to $In_xAl_{1-x}As$ graded buffers (~7.3 nm). While ideal, low-mismatched InAsP was achieved with only a low threading dislocation density present, the InAlAs graded buffers showed evidence for phase decomposition, which was related to the more pronounced surface roughness, and presence of defect structures within the $In_{0.69}Ga_{0.31}As$ overlayer. The impact on devices, however, was found to be manifested primarily in high carrier recombination rates at interfaces, which results from the increased surface roughness for devices grown on InAlAs. In contrast, devices grown on InAsP anion buffers were found to be of high quality. These results and the self-consistency among device, material, and growth properties indicate that III–V graded buffers grown by MBE which utilize the anion sublattice for controlling the lattice constant may be fundamentally superior for III–V metamorphic devices grown on InP.

ACKNOWLEDGMENTS

The authors would like to thank D. M. Wilt, NASA Glenn Research Center, Cleveland, Ohio for technical discussions. This work is supported in part by National Science Foundation (Focused Research Group) under Grant Nos. DMR-0076362 and DMR-0313468.

[1] Y. H. Xie, Mater. Sci. Eng., R. **25**, 89 (1999).

[2] M. T. Bulsara, V. Yang, A. Thilderkvist, E. A. Fitzgerald, K. Haüsler, and K. Eberl, J. Appl. Phys. **83**, 592 (1998).

[3] A. Y. Kim, M. E. Groenert, and E. A. Fitzgerald, J. Electron. Mater. **29**, L9 (2000).

[4] H. Q. Zheng, K. Radhakrishnan, H. Wang, K. H. Yuan, S. F. Yoon, and G. I. Ng, Appl. Phys. Lett. **77**, 869 (2000).

[5] T. P. Chin, H. Q. Hou, C. W. Tu, J. C. P. Chang, and N. Otsuka, Appl. Phys. Lett. **64**, 2001 (1994).

[6] A. Y. Kim, W. S. McCullough, and E. A. Fitzgerald, J. Vac. Sci. Technol. **17**, 1485 (1999).

[7] K. Radhakrishnan, K. Yuan, and H. Q. Zheng, Solid-State Electron. **46**, 877 (2002).

[8] K. Yuan, K. Radhakrishnan, H. Q. Zheng, and S. F. Yoon, Mater. Sci. Semicond. Proc. **4**, 641 (2001).

[9] K. C. Hwang, P. C. Chao, C. Creamer, K. B. Nichols, S. Wang, D. Tu, W. Kong, D. Dugas, and G. Patton, IEEE Electron Device Lett. **20**, 551 (1999).

[10] S. Bollaert, Y. Cordier, V. Hoel, M. Zaknoune, H. Happy, S. Lepilliet, and A. Cappy, IEEE Electron Device Lett. **20**, 123 (1999).

[11] J. C. P. Chang, J. Chen, J. M. Fernandez, H. H. Wieder, and K. L. Kavanagh, Appl. Phys. Lett. **60**, 1129 (1992).

[12] S. A. Ringel *et al.*, Prog. Photovoltaics: Res Technol. **10**, 417 (2002).

[13] M. K. Hudait, Y. Lin, M. N. Palmisiano, and S. A. Ringel, IEEE Electron Device Lett. **EDL-24**, 538 (2003).

[14] M. W. Wanlass, J. J. Carapella, A. Duda, K. Emery, L. Gedvilas, T. Moriarty, S. Ward, J. D. Webb, and X. Wu, Proceedings 4th NREL Conference on TPV Generation of Electricity 1999, Vol. 460, p. 132.

[15] N. S. Fatemi *et al.*, Proceedings 4th NREL Conference on TPV Generation of Electricity 1999, Vol. 460, p. 121.

[16] C. S. Murray, F. Newman, S. Murray, J. Hills, D. Aiken, R. Siergiej, B. Wernsman, and D. Taylor, *29th IEEE Photovoltatic Specialy Conference* (IEEE, New York, 2002), p. 888.

[17] M. K. Hudait, C. L. Andre, O. Kwon, M. N. Palmisiano, and S. A. Ringel, IEEE Electron Device Lett. **23**, 697 (2002).

[18] M. K. Hudait, Y. Lin, D. M. Wilt, J. S. Speck, C. A. Tivarus, E. R. Heller, J. P. Pelz, and S. A. Ringel, Appl. Phys. Lett. **82**, 3212 (2003).

[19] G. Hollinger, D. Gallet, M. Gendry, C. Santinelli, and P. Viktorovitch, J. Vac. Sci. Technol. B **8**, 832 (1990).

[20] J. M. Moiser, M. Bensoussan, and F. Honzay, Phys. Rev. B **34**, 2018 (1986).

[21] V. Swaminathan and A. T. Macrander, *Materials Aspects of GaAs and InP Based Structures* (Prentice Hall, Englewood Cliffs, N.J., 1991).

[22] M. A. G. Halliwell, Adv. X-Ray Anal. **33**, 61 (1990).

[23] B. R. Bennett and J. A. Delalamo, J. Electron. Mater. **20**, 1075 (1991).

[24] I. Vurgaftman, J. R. Meyer, and L. R. Ram-Mohan, J. Appl. Phys. **89**, 5815 (2001).

[25] W. E. Hoke, P. J. Lemonias, J. J. Mosca, P. S. Lyman, A. Torabi, P. F. Marsh, R. A. McTaggart, S. M. Lardizabal, and K. Hetzler, J. Vac. Sci. Technol. B **17**, 1131 (1999).

[26] A. S. Brown, U. K. Mishra, C. S. Chou, C. E. Hooper, M. A. Melendes, M. Thompson, L. E. Larson, S. E. Rosenbaum, and M. J. Delaney, IEEE Electron Device Lett. **10**, 565 (1989).

[27] V. Krishnamoorthy, Y. W. Lin, L. Calhoun, H. L. Liu, and R. M. Park, Appl. Phys. Lett. **61**, 2680 (1992); D. I. Westwood and D. A. Woolf, J. Appl. Phys. **73**, 1187 (1993).

[28] R. S. Goldman, H. H. Wieder, and K. L. Kavanagh, Appl. Phys. Lett. **67**, 344 (1995).

[29] D. Morris, Q. Sun, C. Lacell, A. P. Roth, J. L. Brebner, M. Simard-Normandi, and K. Rajan, J. Appl. Phys. **71**, 2321 (1992).

[30] R. S. Goldman, H. H. Wieder, K. L. Kavanagh, K. Rammohan, and D. H. Rich, Appl. Phys. Lett. **65**, 1424 (1994).

[31] P. M. Asbeck, C.-P. Lee, and M.-C. F. Chang, IEEE Trans. Electron Devices **ED-31**, 1377 (1984).

[32] D. C. Radulescu, G. W. Wicks, W. J. Schaff, A. R. Calawa, and L. F. Eastman, J. Appl. Phys. **62**, 954 (1987).

[33] T. Okada, R. V. Kruzelecky, G. C. Weatherly, D. A. Thompson, and B. J. Robinson, Appl. Phys. Lett. **63**, 3194 (1993).

[34] T. Marschner, M. R. Leys, H. Vonk, and J. H. Wolter, Physica E (Amsterdam) **2**, 873 (1998).

[35] S.-W. Ryu, H.-D. Kim, S.-K. Park, W. G. Jeong, and B.-D. Choe, Jpn. J. Appl. Phys., Part 1 **36**, L79 (1997).

[36] E. A. Fitzgerald, G. P. Watson, R. E. Proano, D. G. Ast, P. D. Kirchner, G. D. Pettit, and J. M. Woodall, J. Appl. Phys. **65**, 2220 (1989).

[37] J. A. Olsen, E. L. Hu, S. R. Lee, I. J. Fritz, J. Howard, B. E. Hammons, and J. Y. Tsao, J. Appl. Phys. **79**, 3578 (1996).

[38] J.-I. Chyi, J.-L. Shieh, J.-W. Pan, and R.-M. Lin, J. Appl. Phys. **79**, 8367 (1996).

[39] H. Ehsani, I. Bhat, R. J. Gutmann, G. Charache, and M. Freeman, J. Appl. Phys. **86**, 835 (1999).

[40] Y. Cordier, D. Ferre, J.-M. Chauveau, and J. Dipersio, Appl. Surf. Sci. **166**, 442 (2000).

[41] J.-M. Chauveau, Y. Androussi, A. Lefebvre, J. Di Persio, and Y. Cordier, J. Appl. Phys. **93**, 4219 (2003).

[42] G. Grenet, E. Bergignat, M. Grendry, M. Lapeyrade, and G. Hollinger, Surf. Sci. **352–354**, 734 (1996).

[43] C. Priester and G. Grenet, Phys. Rev. B **61**, 16029 (2000).

[44] J.-M. Chauveau, Y. Cordier, H. J. Kim, D. Ferre, Y. Androussi, and J. Di Persio, Cryst. Growth **251**, 112 (2003).

[45] T. J. Coutts, Renewable Sustainable Energy Rev **3**, 77 (1999).

[46] R. R. Siergiej *et al.*, Proceedings 5th NREL Conference on TPV Generation of Electricity 2003, Vol. 653, p. 414.